Electronic Supplementary Material (ESI) for Soft Matter.

Repulsive van der Waals forces enable Pickering emulsions with non-touching colloids

Nina A. Elbers, Jessi E. S. van der Hoeven,
D. A. Matthijs de Winter, Chris T. W. M. Schneijdenberg,
Marjolein N. van der Linden, Laura Filion, Alfons van Blaaderen

Supplementary Information

SI Methods

Particles

PMMA particles were synthesized using dispersion polymerization, and were sterically stabilized by a so-called comb-graft steric stabilizing layer formed by poly(12-hydroxystearic acid) (PHSA) grafted onto a backbone of PMMA (PHSA-g-PMMA) [1]. This stabilizer was covalently bound to the particles during a 'locking' step, resulting in positively charged particles [1]. The particles were washed with hexane (p.a., Merck) to remove any unreacted species. Unless indicated otherwise, a batch of locked PMMA particles (2.8 μm in diameter, 3% polydispersity as determined by Static Light Scattering) was used that was covalently labeled with the fluorophore rhodamine isothiocyanate (RITC). Only in one experiment (indicated) unlocked (negatively charged) PMMA particles were used (2.9 μm in diameter, 2% polydispersity as determined by Static Light Scattering), which were dyed with 7-nitrobenzo-2-oxa-1,3-diazol (NBD) [1].

Suspensions

Dry PMMA particles were dispersed in cyclohexyl bromide (CHB, Sigma-Aldrich) that was purified prior to use. This was done by adding activated alumina to it (Al_2O_3; 58 Å, ~150 mesh, Sigma-Aldrich), followed by molecular sieves (4 Å, 10-18 mesh, Acros Organics) until the conductivity was below 80 pS/cm. Dilute suspensions were prepared in CHB or CHB-decalin (27.2 wt%, Sigma-Aldrich) with a 3D particle volume fraction of η=0.001-0.02 (no bulk particles were typically observed in a 2D-setup at $\eta \leq 0.006$), η=0.02 (for capillary studies, 0.1x2-mm VitroCom capillaries) and η=0.01 (for microelectrophoresis). In some studies tetrabutylammonium bromide salt (TBAB, ≤99%, Fluka) was added from a saturated (~300 μM) TBAB stock solution in CHB that was equilibrated for 2 weeks. All oil dispersions were equilibrated for 1 day prior to use. Interfaces were formed using either pure Millipore water, dyed water (Fluorescein isothiocyanate, FITC, Sigma-Aldrich) or salt water (NaCl, ≤99%, Baker, stock solution 0.1 M or TBAB-water, stock solution 0.5 M).

Emulsion preparation

For TBAB-induced particle dislodgement from emulsions, PMMA suspensions were prepared in CHB-decalin (32 wt%, such that $\rho_{PMMA} > \rho_{oil} > \rho_{water}$) at a 3D volumefraction of η=0.024. Hereafter 5.2 vol% of water (containing 1 μM dye; Alexa Fluor®488 biocytin, Lifetechnologies) was added and the sample was homogenized (MS2 minishaker IKA, 2 minutes at 2500 rpm). Imaging was done in 0.1x2-mm capillaries (VitroCom). Macroscopic phase separation was performed in 3x3-mm capillaries (VitroCom), hydrophobized with hexamethyldisilazane (HMDS, SigmaAldrich) using the procedure described in Ref. [2].

For cryo-FIB-SEM studies on emulsions, particle suspensions at a volume fraction η=0.051 in pure CHB were mixed with 10.4 vol% dyed water (Alexa

Fluor®488 biocytin) and homogenized (MS2 minishaker IKA, 1 minute) and sonicated (Branson 8510, 20 seconds). Both the TBAB-induced dislodgement studies as well as the cryo-FIB-SEM studies were performed with freshly prepared emulsions ($\leq$2 days old).

2D-setup

To hydrophobize the bottom glass substrate in the home-built 2D-setup (Figure S1A), a glass slide (24x24 mm, Thermo scientific, Menzel-Glaser, No.1) was washed with soap (Liqui Nox, Alconox) and Millipore water, and coated by an adsorbed layer of Teflon®AF1600 amorphous fluoroplastics (DuPont [3]) using a dipcoater (1-2 mm/s, based on a NEFF WIESEL linear drive unit). The outer cylinder (20 mm diameter) was glued to this glass slide with UV-curing optical adhesive (Norland no. 68). The inner cylinder (8 mm diameter) was made hydrophilic by piranha treatment, and loosely positioned on top of the slide to avoid contact between CHB and any glue. The water phase (sometimes FITC dyed) was added first, followed by positioning $\sim$2 μL of particle suspension on the bottom glass slide by intersecting the aqueous phase. The system was left to equilibrate for at least one hour and drift was minimized by sealing the system with a glass cover slide. Time averaged radial distribution functions g(r) were obtained from the time-series (2 frames/minute) after equilibration, using the IDL-tracking code of Crocker and Weeks [4].

Electrical conductivity measurements

The electrical conductivity (D) in the oil phase (pure CHB or CHB-decalin 27 wt%), was measured using a model 627 conductivity meter (Scientifica, East Sussex, UK) and a 4 mL cup-type probe. At TBAB concentrations c=1-300 μM, a CDM230 conductivity meter was used (Radiometer Analytical). By applying Waldens rule [1, 5, 6, 7] ($\Lambda_0^{rev}\eta_0^{rev}$=$\Lambda_0\eta_0$ with Λ_0^{rev}, η_0^{rev}, Λ_0 and η_0 are the limiting molar conductivity and solvent viscosity in the reference solvent (ethanol or water) and the solvent of interest, respectively), the ionic strength c_i=D/Λ_0 and the Debye length $\kappa^{-1} = (8\pi\lambda_B c_i)^{-1/2}$ were estimated.

Electrophoretic mobility measurements

The particle mobility profiles, and particle charge number Z (obtained from the measured mobility), were determined for the locked PMMA colloids in pure CHB and CHB-decalin 27 wt%, with or without TBAB (c=1-300 μM) using the microelectrophoresis procedure described in Ref. [1]. Typical DC electric field strengths were chosen between 2.8 and 3.6 V mm^{-1}. The particle charge Z of the unlocked PMMA particles in CHB-decalin (20 wt%) was already reported in Ref [1]. In the presence of TBAB, the mobility profiles sometimes became asymmetric due to an unequal coverage of particles at the opposing capillary walls, caused by a collapse in the long-range interparticle repulsion. Here, the absence of well-defined stationary planes allowed us to only determine the sign of

the particle charge from the direction of the particle's electrophoretic motion, and not the charge Z itself. Sample cells consisted of 0.1x2-mm capillaries (VitroCom) that contained two electrodes formed by two 50 μm-diameter nickel alloy wires (T2 thermocouple alloy wire, Goodfellow) bent into a 90 ° angle, at the opposing ends.

Confocal Microscopy

Confocal studies were performed on a horizontal, inverted Leica TCS-SP2 confocal microscope, apart from microelectrophoresis and macroscopic phase separation studies for which a Nikon C1 was used in a vertical position. The fluorescent dyes FITC, NBD and Alexa-488 were excited at 488 nm, and RITC at 532 nm or 543 nm. The objectives used were: 50x air NA 0.55 HXPL Fluotar (for the 2D-setup), 20x air NA 0.7 HC PLAN APO (for macroscopic phase separation) and 100x oil immersion NA 1.4 or 63x oil immersion NA 1.4 Leica, both confocal objectives (for all other studies).

Cryo-FIB-SEM tomography

The emulsion was kept static for 30 min, resulting in a concentrated phase of dispersed water droplets due to creaming. Subsequently, a small volume ($\sim$5 μL) was pipetted in a hollow copper rivet (1 mm inner diameter). The bottom of the rivet was sealed with Tissue-Tek (Agar Scientific), stopping the droplet from running through the rivet. A second rivet was placed upside down on top of the rivet and the entire ensemble was plunge-frozen in liquid nitrogen. Once frozen, the ensemble was transferred to the cryo-preparation chamber (PP2000, Quorum Technologies) under vacuum conditions.

In the cryo-preparation chamber, the top rivet was broken off with a cold knife, creating a freeze-fracture surface of the concentrated emulsion [8]. Next, the surface was sputter coated with platinum and the temperature of the sample was balanced with a FIB-SEM cryo-stage ($-160\,^{\circ}$C) prior to the transfer into the cryo-FIB-SEM (Nova Nanolab 600 Dualbeam, FEI Company).

The area of interest was selected from SEM images. Prior to FIB-milling, a protective layer of platinum deposition was applied [9]. An additional advantage is the electrically conductive nature of the deposited layer, which prevents image drift from charging of the surface.

A cross section was prepared with the FIB, as well as a fiducial marker next to the area of interest. The fiducial marker was used for alignment purposes by both the FIB and the SEM during the automated FIB-SEM tomography routine. The FIB-SEM tomography routine was a sequence of FIB milling and SEM imaging. The FIB removed a slice of material and the SEM imaged the resulting cross section.

Two samples were investigated, and from each sample one FIB-SEM tomography series was used in this study for further analysis. One series was set up with a slice thickness of 100 nm and another with a slice thickness of 50 nm.

Multiple images were recorded with varying magnifications. The highest magnification resulted in series of images with a horizontal pixel dimension of 2.5 nm. The imaging mode was backscattered electron (BSE), which allowed distinguishing the water phase from the oil and PMMA phases by gray value. An additional advantage of the BSE imaging mode was the reduction of charging artifacts in the image.

Cryo-FIB-SEM tomography post-analysis

The structures visible in the series of SEM images were reconstructed in 3D. The images were aligned using the free image processing software package Fiji [10] (StackReg plugin). The FIB cross section was tilted with a 38 ° angle with respect to the SEM imaging plane (XY' plane and XZ plane, respectively in Figure S6A). As a result, the SEM image had to be stretched by a factor $1/\cos(38\,^\circ)$ along Z (horizontal) such that the real dimensions were obtained [11]. In addition, the 3D reconstruction software (IMOD, version 4.7.8; Boulder Laboratory) assumed a slice orientation perpendicular to the surface (XY plane in Figure S6A), which is obtained by compressing the same axis by a factor of $\sin(38\,^\circ)$. The combination of both steps results in a foreshortening by a factor $\tan(38\,^\circ)$, i.e. $Y{=}Z\tan(38\,^\circ)$ [11]. Note that this correction was also accompanied by an increase of the pixel size along this Y axis by the same factor, which will be corrected below. Finally, to simplify the analysis, the image was rotated such that the interface was perpendicular to the x axis. This was again done using the program Fiji.

After correcting the aspect ratio of the pixels of the SEM images, the boundaries of the structures of interest (water droplets and PMMA particles) were identified in each 2D slice. Two methods were used for this. The first was based on fitting a pixel intensity profile with a Gaussian curve. The pixel intensity profile was obtained from an average over 5 (horizontal) rows of pixels. The surface positions in the image were related to the full width at half maximum of the peaks (Figure S6B). Unfortunately, the region of closest approach could not be fitted because of the absence of a strong change in pixel intensity. However, by using a polynomial fit (typical example given in Figure S6C), in the latter case resulting in an extrapolation, a continuous surface profile was obtained. An overlay onto the original image was always used as a visual check (Figure 5E and Figure S6D). The minimum distance between the polynomial functions in the image series formed an estimate for the distance h_0 and the fit itself resulted in the surface coordinates. Finally we used Mathematica (Wolfram, version 10) to reconstruct the 2D polynomial fits into a 3D properly scaled image.

The second method determined the boundaries of the particle and oil-water interface, in each 2D slice, using the Canny edge detector routine in Mathematica. The Canny edge detector had three input parameters: the pixel range in the x and y directions (which we denote r_x, and r_y respectively) and a threshold t_r. For the reconstruction shown in Figure 5I, $r_x = r_y = 18$ and the threshold was $t_r = 0.000725$, which was the optimal parameter set we found, e.g. the edges were clearest and there was least noise in the background. However, as shown

in Figure S7A the position of the edges (shown in red for the above mentioned parameters) was not significantly affected by these parameters: specifically, extreme parameter choices such as 25,25,0.0005 (blue) and 12,12,0.001 (green) (r_x, r_y, t_r, respectively) result in similar edges. The edges associated with the particle and interface (Figures S7B-P) were extracted and fitted to polynomials between order 2-12. Finally, as in the previous case, we reconstructed the system in 3D.

Image charge attractions

As was already reported in Ref. [5], image charge attractions arise when a particle with charge Z, dispersed in an oil medium with a dielectric constant ϵ_m, approaches the interface of a conductor. In the present study it was the water phase that formed the conducting phase, because of the (much) higher dielectric constant and (assumed) relatively high conductivity. An expression for the image charge attraction [12], which contains a small correction compared to the expression mentioned in Ref. [5], is:

$$V(d) = \frac{Z}{\epsilon_m \epsilon_0} \left(\frac{Q}{d} + \frac{Za}{2(a^2 - d^2)} \right) \tag{1}$$

Here, the conducting (water) phase is taken as a sphere with radius a, d is the distance of the colloid from the droplet center, Q is the charge of the water droplet (here taken of the same sign), and ϵ_0 is the dielectric permittivity of vacuum.

Hamaker constant

Unfortunately, for the exotic oil CHB, we do not know the full dielectric spectrum over all imaginary frequencies ($i\nu_n$). Before proceeding, we do want to point out that we are aware that these data are required for reliable predictions on any repulsive van der Waals interactions in our system [13, 14, 15, 16, 17, 18, 19, 20, 21]. However, an indication for the possible existence of a repulsive force can be derived using Lifshitz's theory that uses the static dielectric constants ($\epsilon(i\nu = 0)$) and refractive indices of the three materials [15, 14]. The values are set to ϵ_w=80 (water) [15], ϵ_m=7.92 (medium, CHB) [22], ϵ_p=2.6 (PMMA) [23], n_D^{25}=1.49345 for CHB [22], n_D^{25}=1.492 for PMMA [23] and n_D^{20}=1.333 for water [24]. Assuming that the absorption frequencies (ν_e) of all materials are the same (set to the value for water [15], 3x10^{15} s^{-1}), the equation for the non-retarded Hamaker constant (equation (2a)) reduces to equation (2c). Even though contributions from the visible and UV frequency region typically dominate the interaction ($A_{\nu>0}$, which might or might not be repulsive), the static term ($A_{\nu=0}$, leading to repulsions because here $\epsilon_w > \epsilon_m > \epsilon_p$) might dominate in our system. First, this is caused by the large differences in $\epsilon(i\nu = 0)$ between water and the oil CHB, which reduces in the visible and UV frequency region ($\epsilon(i\nu > 0)$) due to the dielectric constant drop for water [15, 14]. Second, the

negative $A_{\nu=0}$ term possibly stands out because of the refractive index match between PMMA and CHB in the visible region which significantly lowers the contribution for $A_{\nu>0}$. With all these assumptions, we can roughly estimate that the negative Hamaker constant (A_{wmp}), resulting in a repulsion, might be of order -0.3 k_BT. We are also aware of the fact that at distances of ∼20 nm retardation has set in and the calculated A_{wmp} is therefore an upper limit.

$$A_{wmp} = \frac{3k_BT}{2} \sum_{n=0}^{\infty}{}' \left(\frac{\epsilon_p(i\nu_n) - \epsilon_m(i\nu_n)}{\epsilon_p(i\nu_n) + \epsilon_m(i\nu_n)} \right) \left(\frac{\epsilon_w(i\nu_n) - \epsilon_m(i\nu_n)}{\epsilon_w(i\nu_n) + \epsilon_m(i\nu_n)} \right), \tag{2a}$$

$$A_{wmp} = A_{\nu=0} + A_{\nu>0}, \tag{2b}$$

$$\begin{aligned} A_{wmp} \approx{}& \frac{3k_BT}{4} \left(\frac{\epsilon_p - \epsilon_m}{\epsilon_p + \epsilon_m} \right) \left(\frac{\epsilon_w - \epsilon_m}{\epsilon_w + \epsilon_m} \right) \\ &+ \frac{3h\nu_e}{8\sqrt{2}} \frac{\left(n_p^2 - n_m^2\right)\left(n_w^2 - n_m^2\right)}{\sqrt{n_p^2 + n_m^2}\sqrt{n_w^2 + n_m^2}\left(\sqrt{n_p^2 + n_m^2} + \sqrt{n_w^2 + n_m^2}\right)} \end{aligned} \tag{2c}$$

SI Results

Effect of adding TBAB salt to the aqueous phase

We would like to mention that experiments were also performed in which TBAB was initially added to the aqueous phase. Also here, ion transport from the water to the oil phase can result in inversion of the PMMA charge which becomes visible by formation of bands of particle aggregates in the oil phase [25]. In agreement with Ref. [25], this typically happened at about 0.2-0.3 M TBAB in water in the current study. Upon addition of 50 mM TBAB to the aqueous phase, not enough to cause charge inversion, instead of particle dislodgement, particles were found to move towards the interface both in a 2D-setup (Figures S2E,F) as well as in the capillaries (Figures S3E,F,L,M). Certainly this is helped by screening of the electrostatic repulsion between the particles and the interface, allowing more particles to enter the interfacial region. Moreover, diffusiophoresis (i.e. particle movement toward the region high in salt) could also be involved [26, 27], explaining this observation as well.

References

[1] M.N. van der Linden, J.C.P. Stiefelhagen, G. Heessels-Gurboga, J.E.S. van der Hoeven, N.A. Elbers, M. Dijkstra, A. van Blaaderen, *Langmuir* **2015**, *31*, 65.

[2] M. Maccarini, M. Himmelhaus, S. Stoycheva, M. Grunze, *Appl. Surf. Sci.* **2005**, 252, 1941.

[3] DuPont, http://www2.dupont.com/KIV/zh_CN/assets/downloads/DuPont_Teflon_AF_Processing_and_Use_K26986_H44015.pdf

[4] J. Crocker, E. Weeks, www.physics.emory.edu/faculty/weeks//idl/download.html.

[5] M.E. Leunissen, A. van Blaaderen, A.D. Hollingsworth, M.T. Sullivan, P.M. Chaikin, *Proc. Natl. Acad. Sci. U.S.A.* **2007**, 104, 2585.

[6] C.P. Royall, M.E. Leunissen, A. van Blaaderen, *J. Phys. Condens. Matter* **2003**, 15, S3581.

[7] A. Yethiraj, A. van Blaaderen, *Nature* **2003**, 421, 513.

[8] G. Desbois, J.L. Urai, C. Burkhardt, M.R. Drury, M. Hayles, B. Humbel, *Geofluids* **2008**, 8, 60.

[9] M.F. Hayles, D.J. Stokes, D. Phifer, K.C. Findlay, *J. Microsc.* **2007**, 226, 263.

[10] Fiji, http://fiji.sc/Fiji.

[11] D.A.M. de Winter, M.N. Lebbink, D.F.W. de Vries, J.A. Post, M.R. Drury, *J. Microsc.* **2011**, 243, 315.

[12] J.D. Jackson, *Classical Electrodynamics* Wiley, 3rd edition **1998**.

[13] I.E. Dzyaloshinskii, E.M. Lifshitz, L.P. Pitaevskii, *Adv. Phys.* **1961**, 10, 165.

[14] V.A. Parsegian, *Van der Waals force: A handbook for biologists, chemists, engineers, and physicists* Cambridge University Press, New York **2006**.

[15] J.N. Israelachvili, *Intermolecular and Surface Forces* Academic Press, second edition, London **1991**.

[16] J.N. Munday, F. Capasso, V.A. Parsegian, *Nature* **2009**, 457, 170.

[17] P.J. van Zwol, G. Palasantzas, *Phys. Rev. A.* **2010**, 81, 062502.

[18] A.A. Feiler, L. Bergstrom, M.W. Rutland, *Langmuir* **2008**, 24, 2274.

[19] S. Lee, W.M. Sigmund, *J. Colloid Interface Sci.* **2001**, 243, 365.

[20] A. Milling, P. Mulvaney, I. Larson, *J. Colloid Interface Sci.* **1996**, 180, 460.

[21] A. Meurk, P.F. Luckham, L. Bergstrom, *Langmuir* **1997**, 13, 3896.

[22] W.M. Heston, E.J. Hennelly, C.P. Smyth, *J. Am. Chem. Soc.* **1950**, 72, 2071.

[23] M.E. Leunissen, *Manipulating Colloids with Charges & Electric Fields* Ph.D. thesis, Utrecht University, The Netherlands, A digital version of this thesis is available at http://www.colloid.nl **2007**.

[24] W.M. Haynes, *CRC Handbook of Chemistry and Physics* 95th Edition, internet version, http://www.hbcpnetbase.com/ **2014-2015**.

[25] M.E. Leunissen, J. Zwanikken, R. van Roij, P.M. Chaikin, A. van Blaaderen, *Phys. Chem. Chem. Phys.* **2007**, 9, 6405.

[26] D. Florea, S. Musa, J.M.R. Huyghe, H.M. Wyss, *Proc. Natl. Acad. Sci. U.S.A.* **2014**, 111, 6554.

[27] B. Abecassis, C. Cottin-Bizonne, C. Ybert, A. Ajdari, L. Bocquet, *Nat. Mater.* **2008**, 7, 785.

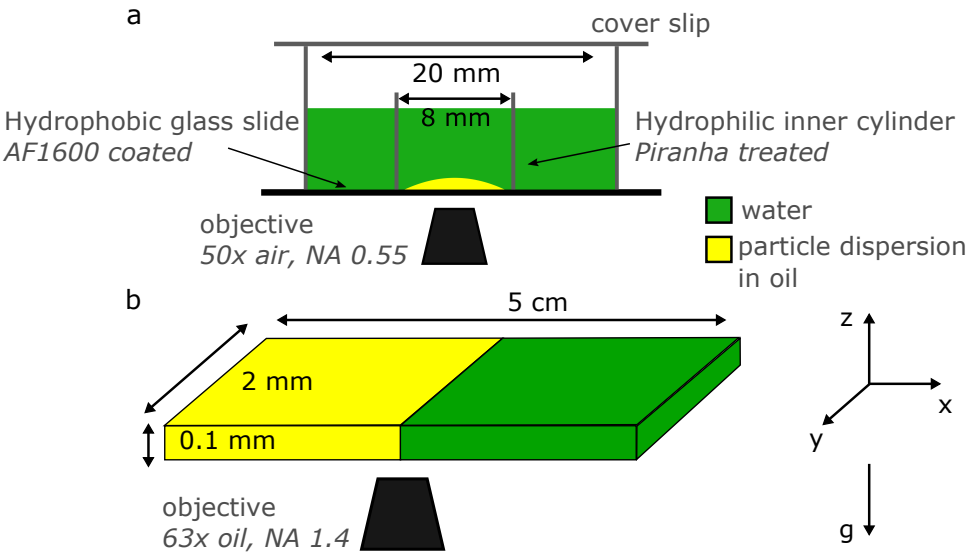

Figure S1: Schematic representation of two different types of setups that were used for the interfacial studies. (A) A home-built 2D-setup, containing an outer cylinder glued on a hydrophobized glass substrate and filled with demineralized water (green). The inner cylinder and vacuum greased coverslip minimized drift effects at the oil-water interface, once a drop of the particle dispersion in oil (yellow) was drop casted onto the glass substrate. The inner cylinder was made hydrophilic by treating it with piranha, in order to minimize wetting by the oil droplet. A long working distance objective was used to image the top of the oil droplet. (B) Capillaries with dimensions 0.1 x 2.0 x 50 mm were half filled with the particle dispersion in oil (yellow) and half filled with an aqueous phase (green) which contained a fluorescent dye in most studies.

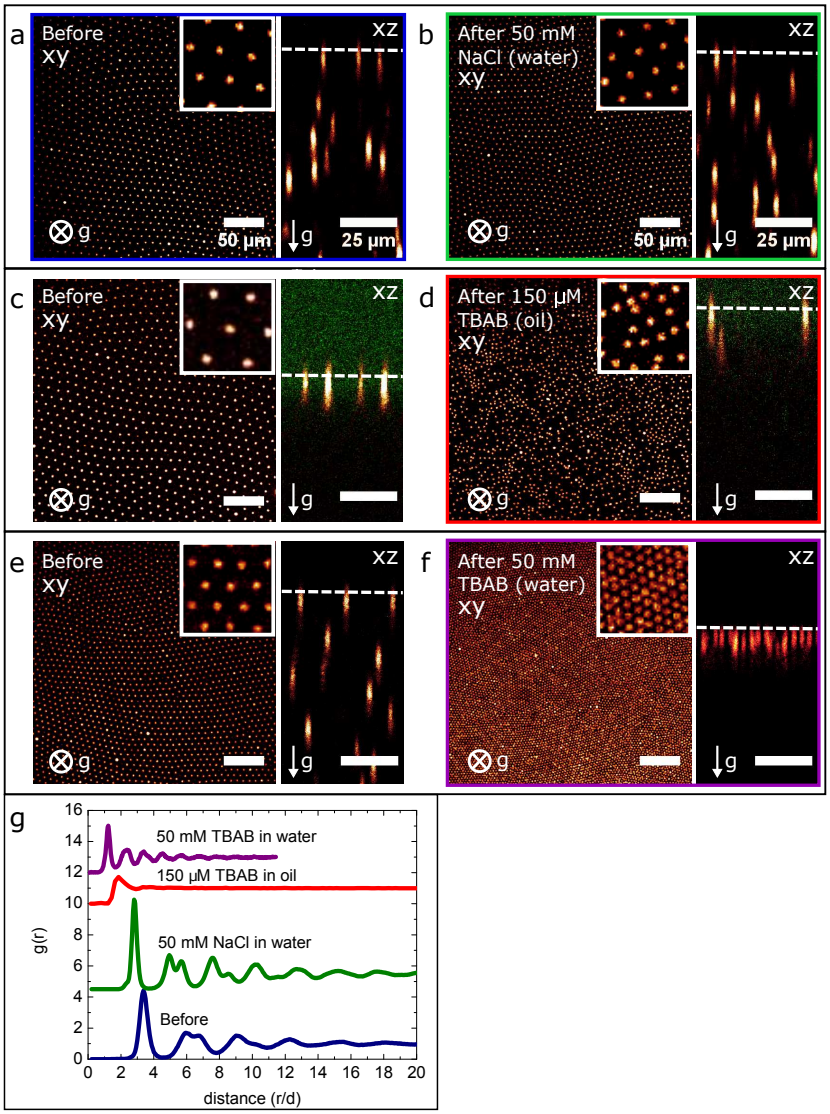

Figure S2: Salt-dependency of the 2D structure and of the interfacial coverage. (A-F) 2D structures of the PMMA particles at a CHB-water interface before adding salt (A,C,E) and the corresponding systems (>15 min) after adding 50 mM NaCl to the aqueous phase (B), 150 μM TBAB to the oil phase (D) and 50 mM TBAB to the aqueous phase (F). The interfacial structure was imaged in the xy-direction (left) and the location of the particles with respect to the interface (dashed line) was imaged in the xz-direction (right). (G) 2D radial distribution functions for the system before adding any salt (corresponding to (A), interparticle spacing 9.4 μm), in presence of 50 mM NaCl added to the aqueous phase (corresponding to (B), interparticle spacing 7.8 μm), 150 μM TBAB added to the oil phase (corresponding to (D), interparticle spacing 5.2 μm) and 50 mM TBAB added to the aqueous phase (corresponding to (F), interparticle spacing 3.4 μm).

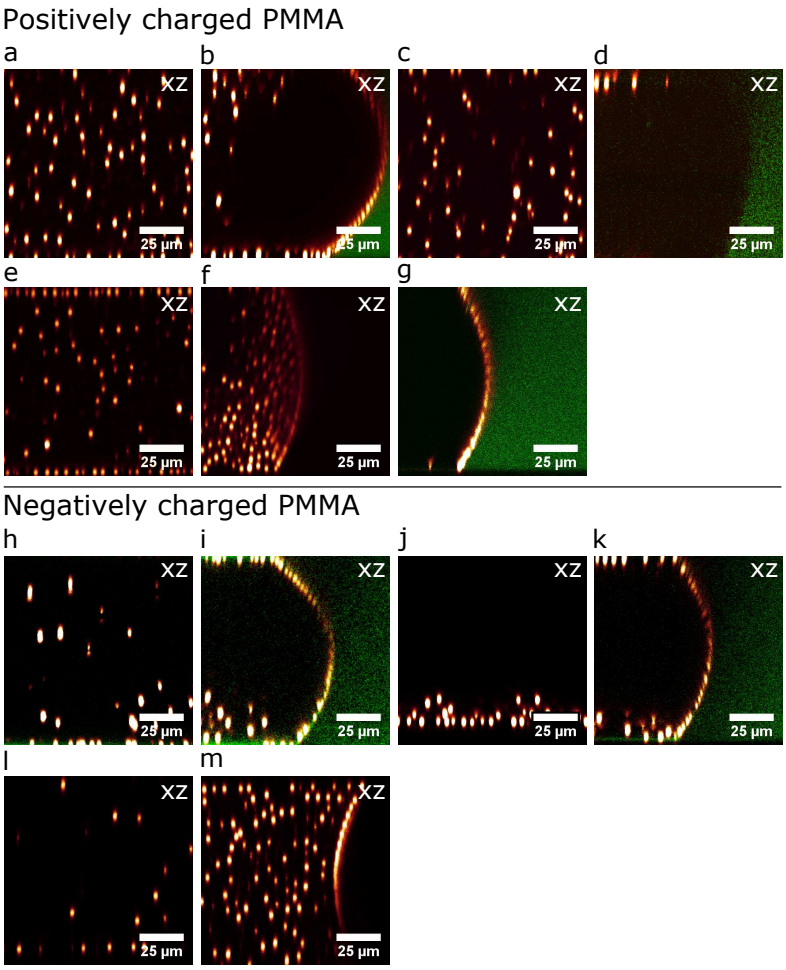

Figure S3: (A-G) Capillary experiments performed with positively charged particles (locked PMMA, charge Z=+930 e determined in CHB). Confocal micrographs taken in bulk oil (A) and at the interface (B) for the system without TBAB salt, as well as in bulk oil (C) and at the interface (D) for the system with 150 μM TBAB in the oil. Confocal micrographs taken in bulk oil (E) and at the interface (F) for the system containing 50 mM TBAB in the aqueous phase, and for the interface (G) at low (0.5 μM) TBAB concentrations in the oil. (H-M) Capillary experiments performed with negatively charged particles (unlocked PMMA, charge Z=-280 e determined in CHB-decalin 20 wt%). Confocal micrographs of the bulk oil (H) and the interface (I) without TBAB salt, as well as of the bulk oil (J) and interface (K) with 180 μM TBAB added to the oil. Confocal micrographs of the the bulk oil (L) and the interface (M) recorded for systems containing 50 mM of TBAB salt in the water phase. All confocal micrographs were recorded in the xz-direction. Water (green) was dyed with FITC. In all experiments, the oil phase was composed of CHB-decalin (27.2 wt%), except for the system in image G which was prepared with pure CHB. Systems were equilibrated beforehand for $\sim$1 h.

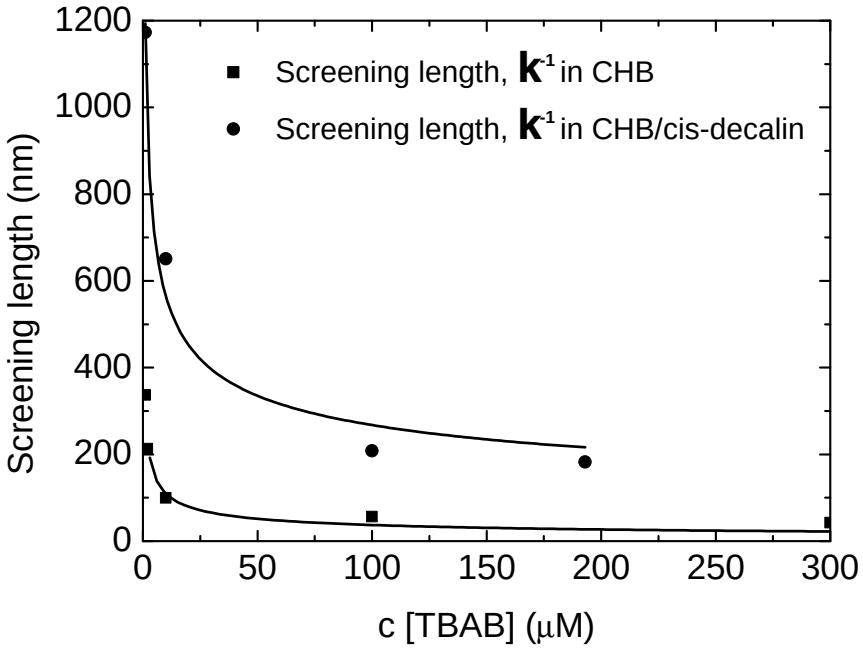

Figure S4: The experimentally determined Debye screening lengths κ^{-1} (nm) as a function of the TBAB concentration in CHB and CHB-decalin (27.2 wt%). The solid lines are guides to the eye.

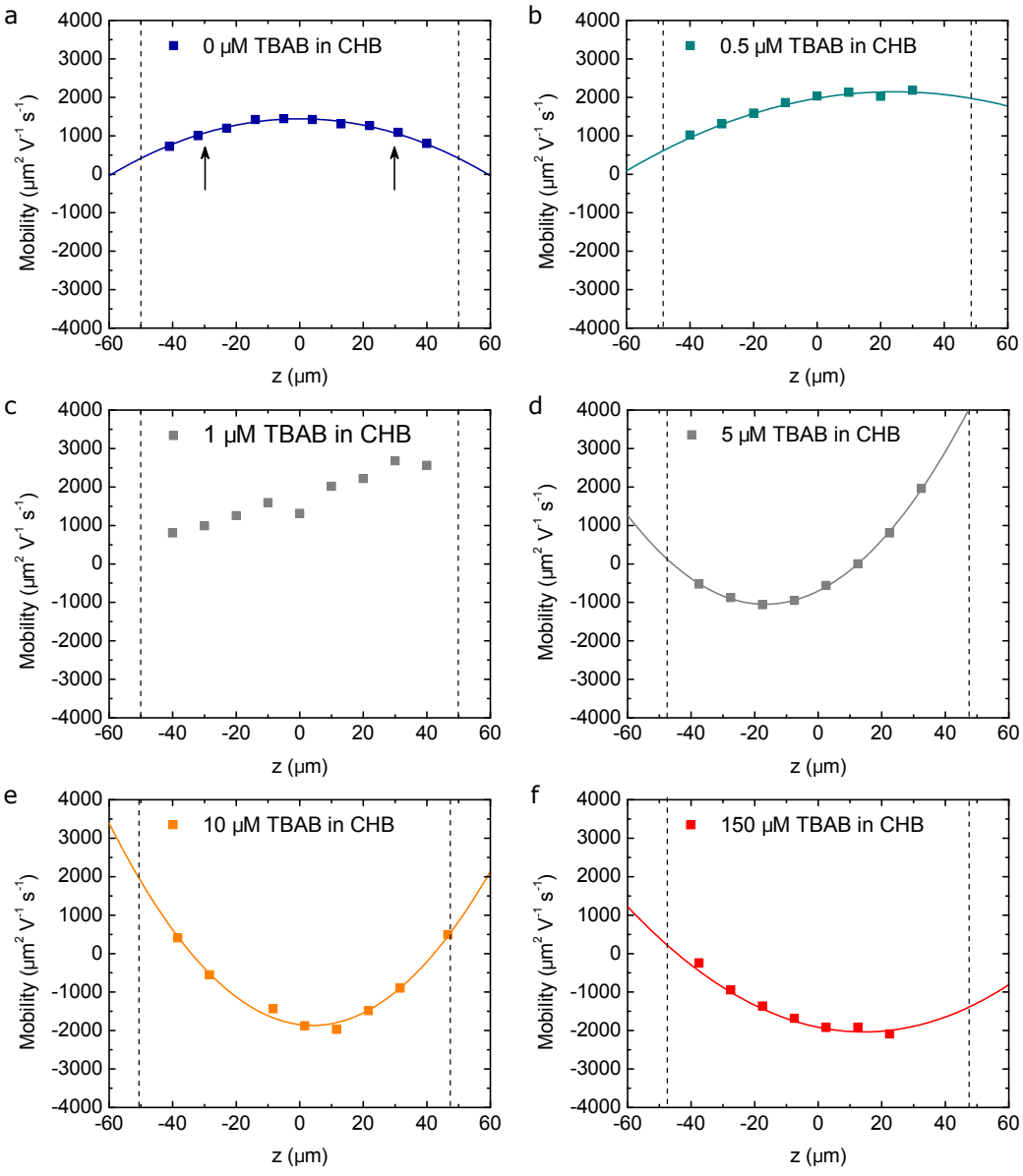
a
0 μM TBAB in CHB
b
0.5 μM TBAB in CHB
c
1 μM TBAB in CHB
d
5 μM TBAB in CHB
e
10 μM TBAB in CHB
f
150 μM TBAB in CHB
Mobility (μm² V⁻¹ s⁻¹)
z (μm)
4000
3000
2000
1000
0
-1000
-2000
-3000
-4000
-60
-40
-20
0
20
40
60

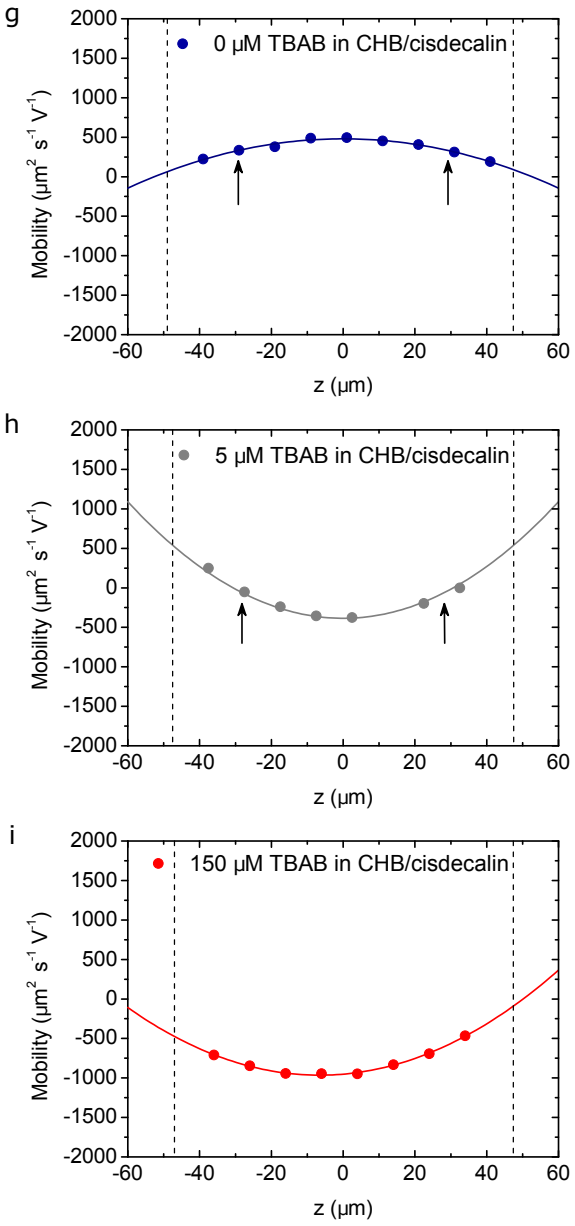

Figure S5: (A-I) Mobility profiles measured in pure CHB at 0 (A), 0.5 (B), 1 (C), 5 (D), 10 (E) and 150 μM TBAB (F) and in CHB-decalin (27.2 wt%) at 0 (G), 5 (H) and 150 μM TBAB (I). The dotted lines indicate the positions of the capillary walls. The stationary planes are indicated with a black arrow for the few cases in which the location could be determined. The DC electric field strengths were 3.6 (A), 2.9 (B), 3.0 (C), 3.0 (D), 2.9 (E), 2.9 (F), 2.7 (G), 3.3 (H) and 2.8 (I) V mm^{-1}.

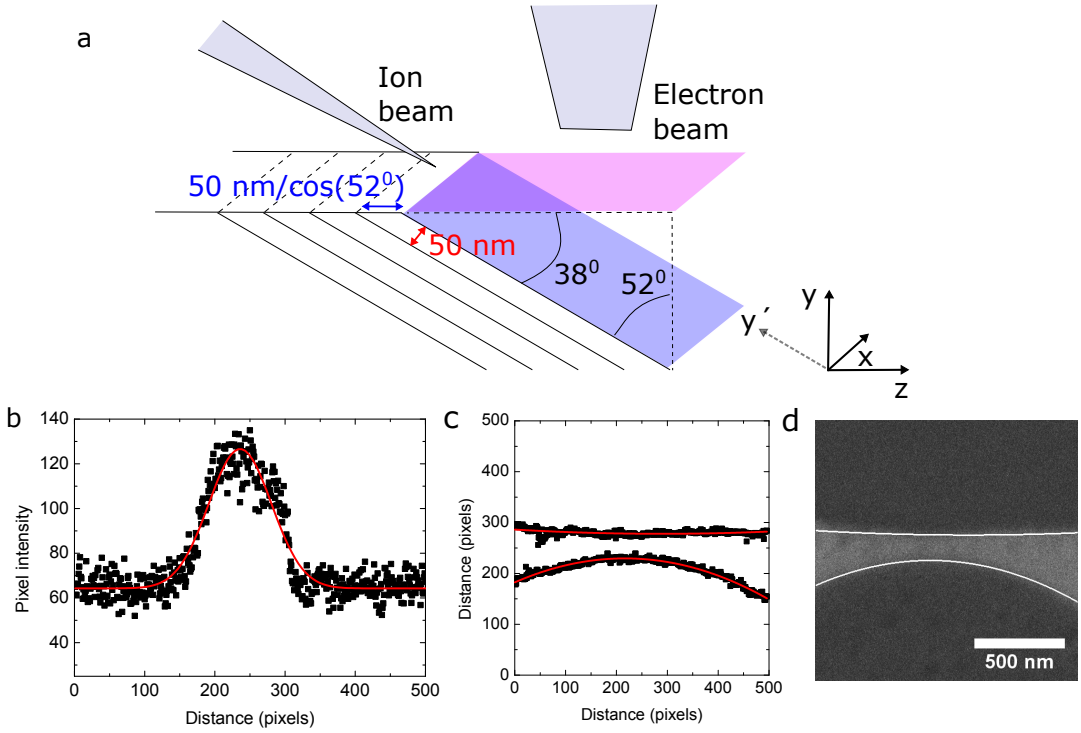

Figure S6: Schematic illustration of the cryo-FIB-SEM setup and results of the interface reconstruction based on fits with polynomial functions. (A) A schematic illustration of the orientations in the cryo-FIB-SEM. (B) The pixel intensity profile of 5 averaged pixel rows (black, scatter) fitted with a Gaussian curve (red, line). Interface positions in the images were related to the full width at half maximum of the Gaussian fits. This step was repeated for all pixel rows in the entire image. (C) The interface positions (black, scatter) were fitted with a polynomial function (red, line). The resulting polynomial functions were used for the 3D reconstruction. (D) An overlay of the polynomial fit onto the original picture, used for a visual check.

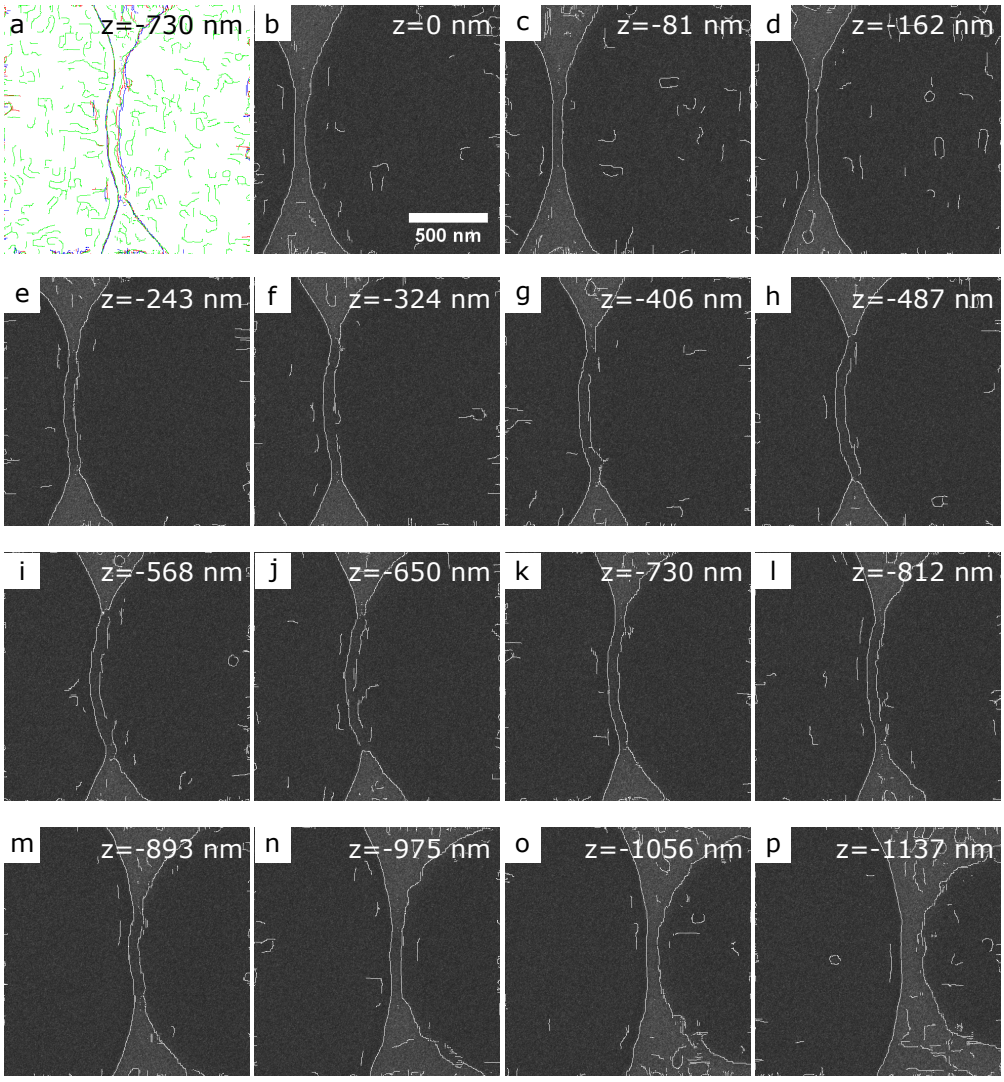

Figure S7: Boundaries of the water droplet and PMMA particle, identified in a FIB-SEM tomography series using an edge detection method. (A) The Canny edge detection method used three input parameters: the pixel range in the x and y directions (r_x, and r_y respectively) and a threshold (t_r). The edges were not significantly affected when changing these parameters from 18,18,0.000725 (red, used in the final reconstruction), 25,25,0.0005 (blue) and 12,12,0.001 (green) (r_x, r_y, t_r, respectively). (B-P) Overlay of the detected surface boundaries on the original FIB-SEM tomography series. The slice thickness (in z) was Δz=50 nm/cos(52 °)=81 nm (see Fig. S6A).